A Robust Algorithm for Microscopic Simulation of Avalanche Breakdown in Semiconductor Devices

Dominic Jabs, Christoph Jungemann, *Senior Member, IEEE*, and Karl Heinz Bach

***Abstract*— Avalanche breakdown can occur during switching of power devices and is difficult to simulate due to its abrupt onset and strong nonlinear behavior. In addition, it severely degrades the numerical robustness of deterministic solvers for the Boltzmann equation (BE), on which the transport simulations are based. A continuation method is therefore introduced, with which robust and efficient simulation of avalanche breakdown is possible. To this end, the generation rate of the secondary electron/hole pairs due to impact ionization is multiplied with a parameter α. Due to this new degree of freedom in the transport equation, voltage as well as current can be specified simultaneously. The final solution is obtained by modifying the voltage or current in such a way that this parameter α becomes one. This approach stabilizes the simulation, improves the numerical robustness of the discrete BE, and avoids divergent solutions. Furthermore, efficient frozen-field simulations of avalanche breakdown become possible. The results are presented for a 1-D p-n junction and a 2-D vertical power MOSFET.**

***Index Terms*— Avalanche breakdown, Boltzmann equation (BE), impact ionization (II), power transistor, spherical harmonic expansion (SHE).**

I. Introduction

IN POWER CIRCUITS, the energy stored in the magnetic field often drives the switching device into avalanche breakdown, when it is turned off [1]. During the transient avalanche breakdown, a large current flows through the power transistor, while a large bias is applied. This leads to the degradation of the semiconductor device by hot carriers, which are either injected into the oxide or generate traps at the Si/SiO_2 interface [2]. A more substantial understanding of these processes might help to design better power devices. In order to approach this subject by device simulation, TCAD tools are required, which can simulate avalanche breakdown and the corresponding hot-carrier processes. Unfortunately, simulation of avalanche breakdown in semiconductor devices is one of the numerically most challenging problems in TCAD. In addition, microscopic modeling of degradation requires the distribution functions of the hot electrons and holes, which can be calculated by the semiclassical Boltzmann equation (BE) [3]. The usual approach to solve the BE is the stochastic Monte Carlo method, which is inherently transient [4]. While this method has many advantages, it is too slow to simulate avalanche breakdown in power transistors. The self-consistent solution to the BE and Poisson equation (PE) requires time steps of a femtosecond or less due to the high carrier densities in the contact regions of the silicon power devices [5], whereas avalanche breakdown in silicon devices needs more than 100 ps to develop for a breakdown voltage of about 40 V. In Fig. 1, the transient solution to a drift–diffusion model [6] is shown for a 1-D abrupt p-n junction with a breakdown voltage of about 37 V for $N_{\mathrm{acc}} = N_{\mathrm{don}} = 3.2 \cdot 10^{16}/\mathrm{cm}^3$ at room temperature. In the first 20 ps after switching the bias from 0 to −39 V, the space-charge region grows and electrons and holes are removed from the p-n junction. Afterwards, the avalanche breakdown starts and it takes more than 200 ps to reach a stationary state. Such time scales are unattainable by Monte Carlo simulations of 2-D power devices, and consequently, different methods, which allow the direct calculation of the stationary state, are required. Another problem is the extreme steepness of the stationary current–voltage (I–V) relation in the case of avalanche breakdown (Fig. 2). Due to the steepness, it is difficult to adjust the bias such that the correct current is achieved.

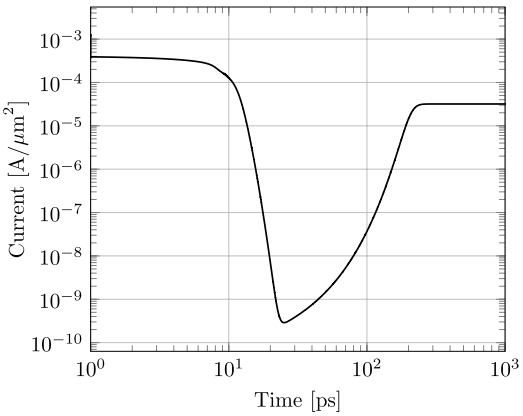

Fig. 1. Transient current of a silicon p-n diode abruptly biased with a reverse bias of 39 V at room temperature by the drift–diffusion model.

Deterministic solvers for the BE based on a spherical harmonic expansion (SHE), which is a deterministic alternative to the Monte Carlo method, have been developed in the past,

Manuscript received March 31, 2015; revised May 11, 2015 and June 3, 2015; accepted June 12, 2015. Date of current version July 21, 2015. This work was supported by the German Federal Ministry for Economic Affairs and Energy under Contract FKZ03ET6003A-I (DriveBattery2015). The review of this paper was arranged by Editor Z. Celik-Butler.

D. Jabs and C. Jungemann are with the Institute of Electromagnetic Theory, RWTH Aachen University, Aachen 52056, Germany (e-mail: jabs@ithe.rwth-aachen.de; cj@ithe.rwth-aachen.de).

K. H. Bach is with Infineon Technologies, Neubiberg 85579, Germany (e-mail: karl-heinz.bach@infineon.com).

Color versions of one or more of the figures in this paper are available online at http://ieeexplore.ieee.org.

Digital Object Identifier 10.1109/TED.2015.2446132

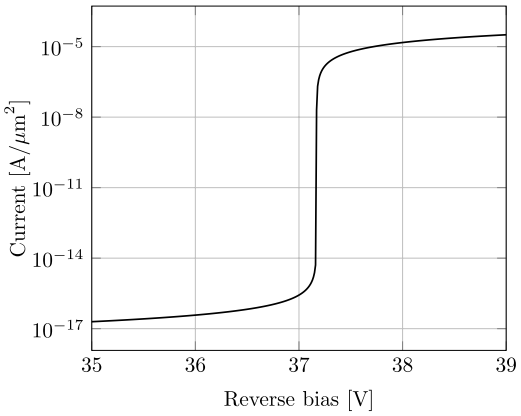

Fig. 2. Current of the silicon p-n diode at room temperature by the drift–diffusion model.

and they directly yield stationary solutions [7], [8]. The necessary effects for the simulation of avalanche breakdown have been included in the approach over time. In [9] and [10], it is described how to model full-band effects, and in [11], self-consistent simulations of electrons and holes were presented. In [12], the first SHE simulations of the avalanche breakdown of a p-n junction occurred, which are still CPU intensive. Resolving the I–V relation in these simulations is difficult, because of its steepness and a lack of the control of the current. In this paper, a new approach is presented, where a current can be predefined, which is much more CPU efficient and leads to a numerically stable discretization of the BE. Section II details this method, and in Section III, the results are shown for the 1-D p-n junction and a 2-D vertical power MOSFET.

II. Simulation Approach

The details of the transport model, the derivation of the discrete BE, and its stabilization can be found in [13]. The model for impact ionization (II) reproduces the experimental results for the II coefficient and quantum yield [14].

This paper focuses on the problems regarding the simulation of avalanche breakdown, which is due to the secondary electrons and holes generated by II. If the potential drop in a p-n junction is large enough to cause an avalanche breakdown, a large current occurs, which leads to a potential drop in the quasi-neutral regions, which in turn reduces the potential drop in the p-n junction limiting the avalanche generation. This is a self-stabilizing process, which requires the self-consistent solution to the BE and the PE. Frozen-field simulations, where the electrostatic potential is fixed and the BE is solved independently from the PE, are therefore instable and can lead to erroneous or divergent solutions. On the other hand, a simultaneous Newton approach of the BE and the PE, which is stable close to the solution, does not converge far from the solution. These problems are due to the divergent behavior of avalanche breakdown, which must be controlled in order to obtain a stable solution to the BE independently from the PE.

Avalanche breakdown is due to the term for the generation of the secondary electron/hole pairs by II, which is therefore split off from the rest of the discrete BE [12]

$$(\hat{B} - \hat{Q})\,\vec{f} = \vec{b} \tag{1}$$

where $\vec{f}$ is the combined discrete distribution function of electrons and holes, $\hat{B}$ is the discrete BE without the II generation term, where the electron and hole parts are no longer coupled by II, and $\hat{Q}$ is the discrete term for the generation of the secondary electron/hole pairs by II. The vector $\vec{b}$ is due to the boundary conditions at the contacts [13]. The BE is linear, because the Pauli principle is neglected. Numerical experiments show that direct solution to this ill-conditioned linear system of equations is difficult not only above, but also somewhat below the breakdown voltage. On the other hand, the linear system without the II generation term ($\hat{B}\,\vec{f} = \vec{b}$) is stable and can be solved directly [13]. Since the matrix $\hat{Q}$ is nonnegative [15], a stable solution can be obtained by an iterative approach [12]

$$\hat{B}\,\vec{f}_k = \hat{Q}\,\vec{f}_{k-1} + \vec{b} \tag{2}$$

with the initial condition $\hat{B}\,\vec{f}_0 = \vec{b}$. Within an iteration step, the generation of secondary particles is fixed to $\hat{Q}\,\vec{f}_{k-1}$ and no unchecked avalanche breakdown can occur. The solution $\vec{f}_k$ at each iteration step results in a new space-charge distribution. Only if the PE is solved with this new space-charge distribution and the matrices $\hat{B}$ and $\hat{Q}$ are rebuilt due to the new potential resulting from the PE, divergent solutions are avoided. As building the matrices and solving the linear system might take hours, a large number of iteration steps are not feasible. Furthermore, it is very difficult to simulate a specific current due to the steep slope of the I–V characteristics at breakdown (Fig. 2).

These problems can be circumvented by a new approach, in which not only the bias but also the current is predefined. A new degree of freedom is introduced in the BE to permit the choice of the current. The generation term is multiplied with a factor α

$$(\hat{B} - \alpha\,\hat{Q})\,\vec{f} = \vec{b} \tag{3}$$

and an equation for the current is added to determine α

$$\vec{c}^{\,T}\,\vec{f} = I_{\mathrm{BD}}. \tag{4}$$

The terminal current is calculated with the linear operator $\vec{c}$, where the terminal is the one for which the current should be equal to the breakdown current I_{BD}. For the given bias conditions and a given breakdown current, this modified BE is solved for the distribution function $\vec{f}$ and the factor α. Thus, α is a result of this system of equations and is calculated in such a way that the current is limited to I_{BD} and can no longer diverge.

Equation (3) is nonlinear due to the product of α and $\vec{f}$ in the generation term, and after the elimination of α, it is given by

$$\vec{f} = \vec{h}(\vec{f}) = \frac{I_{\mathrm{BD}} - \vec{c}^{\,T}\,\vec{f}_0}{\vec{c}^{\,T}\,\hat{B}^{-1}\,\hat{Q}\,\vec{f}}\,\hat{B}^{-1}\,\hat{Q}\,\vec{f} + \vec{f}_0 \tag{5}$$

with $\hat{B}\vec{f}_0 = \vec{b}$. This equation can be solved by a fixed-point iteration ($k = 1, 2, \ldots$)

$$\hat{B}\vec{g}_k = \hat{Q}\vec{f}_{k-1} \tag{6}$$

$$\alpha_k = \frac{I_{\mathrm{BD}} - \vec{c}^{\,T}\vec{f}_0}{\vec{c}^{\,T}\vec{g}_k} \tag{7}$$

$$\vec{f}_k = \alpha_k\vec{g}_k + \vec{f}_0. \tag{8}$$

The linear system in (6) is numerically stable due to the favorable properties of the matrix $\hat{B}$ similar to (2).

For the solution $\vec{f}_\infty = \vec{h}(\vec{f}_\infty)$, the Jacobian matrix $[\hat{J}]_{ij} = \partial h_i/\partial f_j$ is given by

$$\hat{J} = \alpha_\infty\left[\hat{I} - \frac{(\vec{f}_\infty - \vec{f}_0)\vec{c}^{\,T}}{\vec{c}^{\,T}(\vec{f}_\infty - \vec{f}_0)}\right]\hat{B}^{-1}\hat{Q} \tag{9}$$

with $I_{\mathrm{BD}} = \vec{c}^{\,T}\vec{f}_\infty$ and $\alpha_\infty = \alpha(\vec{f}_\infty)$. $\hat{I}$ is the identity matrix. $\vec{c}$ is a left eigenvector, and $\vec{f}_\infty$ is a right eigenvector of this Jacobian matrix for the eigenvalue zero

$$\vec{c}^{\,T}\hat{J} = 0, \quad \hat{J}\vec{f}_\infty = 0. \tag{10}$$

Close to the solution, the fixed-point iteration is given up to the first order in $\delta\vec{f} = \vec{f} - \vec{f}_\infty$ by

$$\delta\vec{f}_k = \hat{J}\delta\vec{f}_{k-1}. \tag{11}$$

Since $\hat{J}\vec{f}_\infty = 0$ holds, $\delta\vec{f}_k$ will be orthogonal to $\vec{f}_\infty$ close to the solution. The excellent convergence behavior of this fixed-point iteration will be demonstrated in the next section.

The fixed-point iteration (6)–(8) can be performed CPU efficiently with a sparse matrix solver. An incomplete LU decomposition is obtained for $\hat{B}$ by the software package ILUPACK [16]. This calculation and the setup of $\hat{B}$, which are both very CPU intensive, are performed only once for a given potential. The linear system in the fixed-point iteration (6)–(8) is solved by a generalized minimal residual method (GMRES [17]), where the ILU of $\hat{B}$ is reused. Solving the linear system with the GMRES takes only a small fraction of the time needed to build $\hat{B}$ and to calculate its incomplete LU decomposition. Thus, the fixed-point iteration does not take much more time than a single step of the iteration in (2).

The fixed-point iteration is embedded in a Gummel loop together with the PE to achieve a self-consistent solution to both equations [18]. The result of this iteration is in general a factor α, which deviates from one. To obtain a physically meaningful solution, $\alpha = 1$ is required. This can be achieved either by varying the corresponding bias or current. Since in degradation experiments, often a current compliance is used, the bias is varied and the current is kept constant. It is empirically found that the pairs of V and α agree well with the relation

$$V = V_{\mathrm{BD}}\,\alpha^\beta \tag{12}$$

where V_{BD} and β are the fixed parameters. This relation (12) can be used to formulate a simple iteration. For a fixed I_{BD} and two different voltages V_1 and V_2 the factors α_1 and α_2 are calculated with the iteration scheme (6)–(8). From these results, the parameter V_{BD} is obtained and a new α is calculated for $V = V_{\mathrm{BD}}$. The resultant α should be already close to one. This procedure is repeated, until α is sufficiently close to one. This approach is a numerical continuation method for the additional factor α [19], where the factor α is implicitly determined by the applied voltage and current. The improved numerical stability is due to the current compliance.

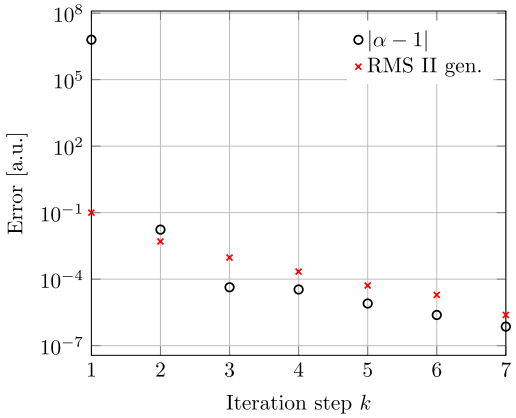

Fig. 3. Convergence of the factor α toward one and the RMS error of the electron II generation rate during the fixed-point iteration for a current of 10 pA/μm^2 and a reverse bias of 37.172 V.

If the whole I–V curve is required and the relationship between current I and bias V is complicated (e.g., snapback), instead of using (12), a different numerical continuation method could be used [19]. The fixed-point iteration with the parameter α is also well suited for piecewise linear continuation. The solution is then the contour line in the current-bias space, for which $\alpha(I, V) = 1$ holds.

Hot-carrier simulations are often performed in the nonself-consistent mode for a frozen electric field because the few hot electrons or holes have a negligible impact on the space charge and, thus, on the potential [20]–[22]. This reduces the CPU time a lot. In the case of avalanche breakdown, this requires the independent solution of the BE, which is possible with the new approach. Thus, nonself-consistent simulations can be utilized also in the case of avalanche breakdown and the described Gummel loop for the BE and PE can be avoided. Instead, the potential is calculated by solving a CPU-efficient transport model without II (e.g., drift–diffusion model), and the BE is solved only once for the given potential.

III. Results

A. p-n Diode

The p-n diode of 5-μm length with the abrupt doping profile of Fig. 6 is simulated with the SHE solver. For a reverse bias of 37.172 V and a current of 10 pA/μm^2, the factor alpha is equal to one. The convergence of the corresponding fixed-point iteration (6)–(8) is shown in Fig. 3. The first value α_1 is very large, because the initial distribution function $\vec{f}_0$ is calculated without II generation of secondary carriers and the saturation current of the diode is many orders of magnitude smaller than the current compliance. In the second step, the error drops by eight orders of magnitude and the factor is already close to one ($\alpha_2 = 0.9828$). This is remarkable, because the solution to the BE changes within one step of the iteration from the one without avalanche

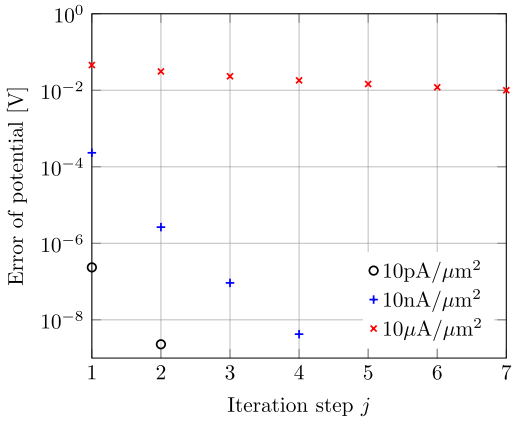

Fig. 4. Maximum change in the potential of the Gummel loop for the BE and PE for three currents and a reverse bias of 37.172 V.

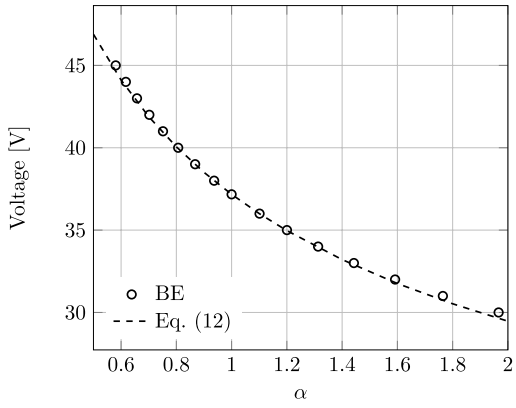

Fig. 5. Reverse bias for the p-n diode as a function of the factor α for a current of 10 pA/μm^2 evaluated by solving the BE (symbols) and (12) with $V_{\mathrm{BD}} = 37.172$ V and $\beta = -0.335$ (dashed line).

breakdown to an already very accurate solution including avalanche breakdown. After seven iterations, the error is less than 10^{-6}. In addition, in Fig. 3, the convergence of the II generation rate of electrons is shown, which demonstrates that not only α shows good convergence. Hence, the fixed-point iteration shows robust and fast convergence.

The nonlinear BE with current compliance is solved self-consistently with the PE by a Gummel loop, which shows excellent convergence for small and medium currents (Fig. 4). The convergence problems associated with the avalanche breakdown do not occur, because the current is fixed. This demonstrates the robustness of the new algorithm. In the case of the smallest current, the potential changes less than a microvolt in the first iteration, and a self-consistent solution to the BE and PE is not necessary. In the case of the largest current, the convergence is slow, but this is similar to the case of the Gummel loop for a forwardly biased p-n junction and the convergence can be improved with standard TCAD methods for this case [23]. As the vertical power nMOSFET in Section III-B is usually not driven into such large currents, because it would be thermally destroyed within a short time, the treatment of such large currents shall not be discussed here.

In Fig. 5, the voltage required for a current of 10 pA/μm^2 is shown as a function of the factor α. The dashed line is

TABLE I

FACTOR α AS A FUNCTION OF THE REVERSE BIAS FOR THE p-n DIODE FOR A CURRENT OF 10 pA/μm^2

i	Bias [V]	α
1	41.0	0.751554
2	40.0	0.806669
3	37.106	1.005331
4	37.17336	0.999893
5	37.17203	0.999998

TABLE II

BREAKDOWN VOLTAGE V_{BD} AS A FUNCTION OF THE CURRENT

Current [A/μm^2]	Bias [V]
10^{-13}	37.17198740
10^{-11}	37.17210360
10^{-8}	37.17210470

the result of (12), and the symbols are the results of the BE. The good agreement implies that the empirical relation in (12) describes the relation between α and the voltage well. With (12), the bias for $\alpha = 1$ is calculated by iteration. The results of this iteration are shown in Table I. The first two voltages are used to initialize the iteration. Although these two values are far away from the final result, the third value is already close to the final result, and after five evaluations, an accurate result is obtained. Thus, starting far away from the final solution does not cause problems, and this result demonstrates how fast convergence can be obtained for avalanche breakdown with this approach.

Table II reveals that due to the steepness of the I–V relation (Fig. 2), this iteration yields a very small change in the breakdown voltages of just 23 μV/decade change in the current.

In the top graph of Fig. 6, the electron and hole densities are shown for the same bias and two different currents, which differ by three orders of magnitude (10 pA/μm^2 and 10 nA/μm^2). The simulations are self-consistent with the PE. Significant differences in the densities are found only in the space-charge region, whereas the majority electron and hole densities in the quasi-neutral regions are (almost) the same and equal to the corresponding doping concentrations. In the bottom graph of Fig. 6, the corresponding II generation rates of holes and electrons are shown, where the results are divided by the current. In the space-charge region, the results for the two currents agree very well, demonstrating that the hot-carrier effects are proportional to the current for these small currents. The deviations in the quasi-neutral regions are due to the fact that the distribution function of the majority carriers in those regions is almost the equilibrium one, which depends only on the particle density and not on the current level. Since the corresponding II generation rates are many orders of magnitude smaller than those in the space-charge region, their impact is negligible. This linear behavior of the hot-carrier effects is not only found for the II generation rate but also in the case of the distribution function itself. In Fig. 7, the energy distribution functions of electrons and holes divided by the corresponding current are shown in the center of the p-n junction; the agreement is so good that the difference is

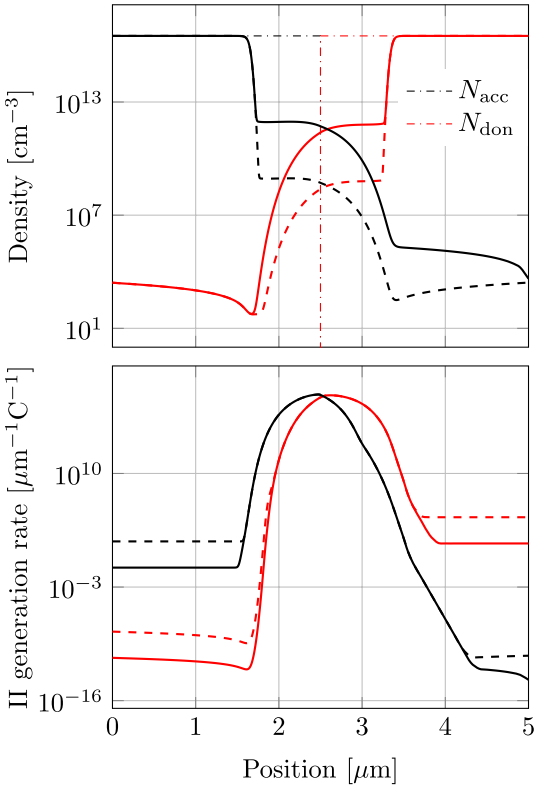

Fig. 6. Electron (red, top graph) and hole (black, top graph) density, and II generation due to electrons (red, bottom graph) and holes (black, bottom graph) at 37.172 V and room temperature for 10 pA/μm^2 (dashed lines) and 10 nA/μm^2 (solid lines). Doping profiles (dashed dotted, top graph).

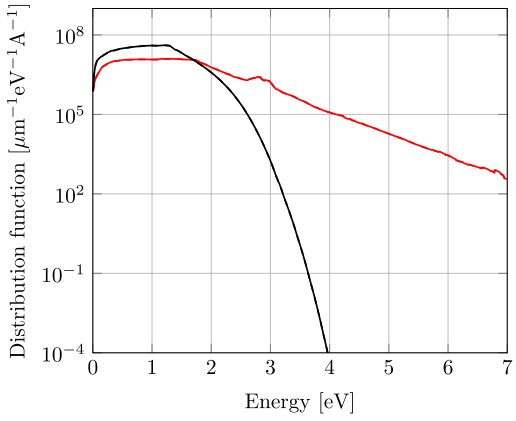

Fig. 7. Energy distribution function for electrons (red) and holes (black) in the middle of the p-n junction ($x = 2.5$ μm) at 37.172 V and room temperature for 10 pA/μm^2 (dashed lines) and for 10 nA/μm^2 (solid lines) scaled with the corresponding current density.

not visible in Fig. 7. This linear behavior in the technically relevant current range allows us to use current levels, which are so low that nonself-consistent simulations can be performed, which are much more CPU efficient.

B. Vertical Power MOSFET

In order to demonstrate that this approach works not only in the case of a rather ideal 1-D p-n diode, we have simulated a vertical power nMOSFET. The 2-D process and device

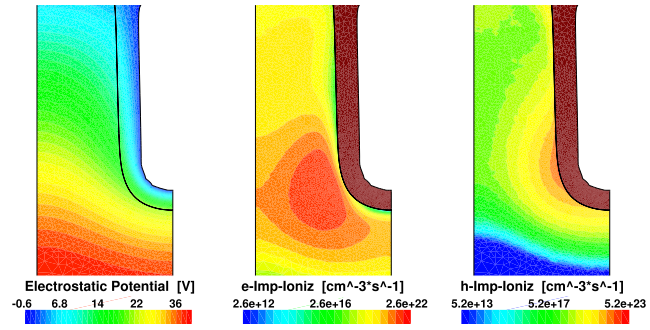

Fig. 8. Potential, electron, and hole II rates in the space-charge region of the vertical power MOSFET for a drain bias of 35.83 and 0 V at all other contacts for a current of 10 pA/μm^2.

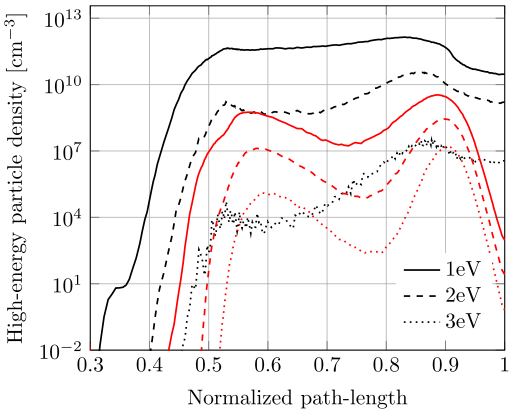

Fig. 9. Density of electrons (red) and holes (black) with energies higher than 1, 2, and 3 eV at a drain bias of 35.83 V and room temperature along the Si/SiO$_2$ interface. The value one of the x-ordinate corresponds to the lower right end of the interface in Fig. 8.

simulations for this device were performed with the Sentaurus TCAD suite [24]. The device structure, grid, doping profile, and electrostatic potential of the drift–diffusion simulation without II were transferred to our code.

The current density was set to 10 pA/μm^2, a value low enough for nonself-consistent simulations, and for a drain/source bias of 35.83 and 0 V at all other contacts, $\alpha = 1$ is obtained. The number of unknown variables of the linear system is 45 million (about 4700 nodes in the real space), and the total CPU time is less than 11 h on a current computer.

The potential and II rates of electrons and holes are shown in Fig. 8 for the space-charge region of the power transistor. The II generation rate of the holes peaks at the Si/SiO$_2$ interface near the bottom of the trench oxide (the brown region in Fig. 8), whereas the peak of the electron II rate is found in the bulk of the device due to the electric field, which repels electrons from the trench. The electron II distribution is therefore more spread out than the hole one, which is concentrated close to the trench interface. Nevertheless, it is possible to calculate the rather low electron and hole distribution functions along the trench interface by our approach, as shown in Fig. 9. Based on these results, device degradation due to the injection of hot electrons and holes into the oxide and generation of traps at the interface could be calculated.

IV. Conclusion

We have demonstrated a new approach based on numerical continuation for the simulation of avalanche breakdown, where the voltage and breakdown current can be specified by introducing a multiplier for the II generation rate of the secondary electron/hole pairs. The new approach is robust and efficient, and the problem of divergent solutions is avoided. It works even in the region of the I–V characteristics, where its slope is steepest, and we have demonstrated for the first time a solution to the BE for avalanche breakdown in a power transistor with a current compliance. In addition, the new approach improves the stability of the BE to such an extent that CPU-efficient frozen-field simulations of avalanche breakdown are possible.

Since in this new approach, voltage and current can be specified, it might also work in the case where the relationship between current and voltage is not invertible and piecewise linear continuation methods could be used. Furthermore, the approach is not limited to the BE, but can also be used, for example, in the case of the drift–diffusion model.

References

[1] K. Fischer and K. Shenai, "Dynamics of power MOSFET switching under unclamped inductive loading conditions," *IEEE Trans. Electron Devices*, vol. 43, no. 6, pp. 1007–1015, Jun. 1996.

[2] A. Acovic, G. La Rosa, and Y.-C. Sun, "A review of hot-carrier degradation mechanisms in MOSFETs," *Microelectron. Rel.*, vol. 36, nos. 7–8, pp. 845–869, 1996.

[3] K. Hess, Ed., *Monte Carlo Device Simulation: Full Band and Beyond*. Boston, MA, USA: Kluwer, 1991.

[4] C. Jacoboni and P. Lugli, *The Monte Carlo Method for Semiconductor Device Simulation*. Vienna, Austria: Springer-Verlag, 1989.

[5] P. W. Rambo and J. Denavit, "Time stability of Monte Carlo device simulation," *IEEE Trans. Comput.-Aided Design Integr. Circuits Syst.*, vol. 12, no. 11, pp. 1734–1741, Nov. 1993.

[6] *GALENE III User's Guide*, 3rd ed., Technische Universität Braunschweig, Braunschweig, Germany, 2006.

[7] A. Gnudi, D. Ventura, G. Baccarani, and F. Odeh, "Two-dimensional MOSFET simulation by means of a multidimensional spherical harmonics expansion of the Boltzmann transport equation," *Solid-State Electron.*, vol. 36, no. 4, pp. 575–581, 1993.

[8] W. Liang, N. Goldsman, I. Mayergoyz, and P. J. Oldiges, "2-D MOSFET modeling including surface effects and impact ionization by self-consistent solution of the Boltzmann, Poisson, and hole-continuity equations," *IEEE Trans. Electron Devices*, vol. 44, no. 2, pp. 257–267, Feb. 1997.

[9] M. C. Vecchi and M. Rudan, "Modeling electron and hole transport with full-band structure effects by means of the spherical-harmonics expansion of the BTE," *IEEE Trans. Electron Devices*, vol. 45, no. 1, pp. 230–238, Jan. 1998.

[10] S. Jin, S.-M. Hong, and C. Jungemann, "An efficient approach to include full-band effects in deterministic Boltzmann equation solver based on high-order spherical harmonics expansion," *IEEE Trans. Electron Devices*, vol. 58, no. 5, pp. 1287–1294, May 2011.

[11] K. Rupp, C. Jungemann, M. Bina, A. Jüngel, and T. Grasser, "Bipolar spherical harmonics expansions of the Boltzmann transport equation," in *Proc. SISPAD*, 2012, pp. 19–22.

[12] D. Jabs and C. Jungemann, "Avalanche breakdown of pn-junctions—Simulation by spherical harmonics expansion of the Boltzmann transport equation," in *Proc. Int. Conf. Simulation Semiconductor Process. Devices (SISPAD)*, Sep. 2014, pp. 173–176.

[13] S.-M. Hong, A.-T. Pham, and C. Jungemann, *Deterministic Solvers for the Boltzmann Transport Equation* (Computational Microelectronics), S. Selberherr, Ed. New York, NY, USA: Springer-Verlag, 2011.

[14] C. Jungemann and B. Meinerzhagen, *Hierarchical Device Simulation: The Monte-Carlo Perspective* (Computational Microelectronics). New York, NY, USA: Springer-Verlag, 2003.

[15] Y. Saad, *Iterative Methods for Sparse Linear Systems*, 2nd ed. Philadelphia, PA, USA: SIAM, 2003.

[16] M. Bollhöfer and Y. Saad, "Multilevel preconditioners constructed from inverse-based ILUs," *SIAM J. Sci. Comput.*, vol. 27, no. 5, pp. 1627–1650, 2006.

[17] Y. Saad and M. H. Schultz, "GMRES: A generalized minimal residual algorithm for solving nonsymmetric linear systems," *SIAM J. Sci. Statist. Comput.*, vol. 7, no. 3, pp. 856–869, 1986.

[18] H. K. Gummel, "A self-consistent iterative scheme for one-dimensional steady state transistor calculations," *IEEE Trans. Electron Devices*, vol. 11, no. 10, pp. 455–465, Oct. 1964.

[19] E. L. Allgower and K. Georg, *Introduction to Numerical Continuation Methods* (Classics in Applied Mathematics), vol. 45. Philadelphia, PA, USA: SIAM, 2003.

[20] J. M. Higman, K. Hess, C. G. Hwang, and R. W. Dutton, "Coupled Monte Carlo-drift diffusion analysis of hot-electron effects in MOSFETs," *IEEE Trans. Electron Devices*, vol. 36, no. 5, pp. 930–937, May 1989.

[21] J. D. Bude and M. Mastrapasqua, "Impact ionization and distribution functions in sub-micron nMOSFET technologies," *IEEE Electron Device Lett.*, vol. 16, no. 10, pp. 439–441, Oct. 1995.

[22] C. Jungemann, S. Yamaguchi, and H. Goto, "On the accuracy and efficiency of substrate current calculations for sub-μm n-MOSFET's," *IEEE Electron Device Lett.*, vol. 17, no. 10, pp. 464–466, Oct. 1996.

[23] S. Selberherr, *Analysis and Simulation of Semiconductor Devices*. Vienna, Austria: Springer-Verlag, 1984.

[24] *TCAD Sentaurus*, G-2012.06 ed., Synopsys Inc., Mountain View, CA, USA, 2012.

Dominic Jabs received the B.Sc. and M.Sc. degrees in physics from RWTH Aachen University, Aachen, Germany, in 2009 and 2011, respectively.

He has been the Chair of Electromagnetic Theory with RWTH Aachen University since 2012. He is focused on physics-based simulation of semiconductor-power devices.

Christoph Jungemann (M'97–SM'06) received the Degree in electrical engineering from RWTH Aachen University, Aachen, Germany.

He became a Professor of Microelectronics with Bundeswehr University, Munich, Germany, in 2006. Since 2011, he has held the Chair of Electromagnetic Theory with RWTH Aachen University.

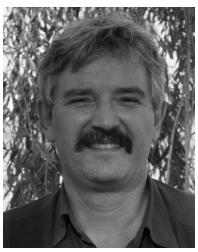

Karl Heinz Bach received the Degree in electrical engineering from RWTH Aachen University, Aachen, Germany.

He joined TEMIC Semiconductor, Heilbronn, Germany, in 1991, where he has been involved in BiCMOS integration. Since 1999, he has been with Infineon Technologies, Munich, focusing on TCAD simulation of advanced CMOS devices with an emphasis on stress impact, and particularly on optimization of power devices with respect to avalanche operation since 2008.